J Mater Sci (2008) 43:933–941
DOI 10.1007/s10853-007-2207-4

Reaction–formation mechanisms and microstructure evolution of biomorphic SiC

Francisco M. Varela-Feria · Joaquín Ramírez-Rico · Antonio R. de Arellano-López · Julián Martínez-Fernández · Mrityunjay Singh

Received: 13 June 2007 / Accepted: 4 October 2007 / Published online: 9 November 2007

Abstract Biomorphic SiC is fabricated by liquid Si infiltration of a carbon preform obtained from pyrolized wood that can be selected for tailored properties. The microstructure and reaction kinetics of biomorphic SiC have been investigated by means of TEM, SEM, EBSD, and partial infiltration experiments. The microstructure of the material consists of SiC and Si and a small fraction of unreacted C. The SiC follows a bimodal size distribution of grains in the micrometer and the nanometer range with no preferential orientation. The infiltration-reaction constant has been determined as 18×10^{-3} s^{-1}. These observations suggest that the main mechanism for SiC formation is solution–precipitation in the first stage of growth. If the pores in the wood are small enough they can be choked by SiC grains that act as a diffusion barrier between Si and C. If that is the case, Si will diffuse through SiC forming SiC grains in the nanometer range.

Introduction

Silicon carbide-based ceramics are important materials for key engineering applications demanding good thermo-mechanical performance and density/properties relationships. However, fabricating bulk SiC-based materials with complex shapes require expensive extrusion, molding, and cutting techniques that are difficult to amortize and prevent the use of these excellent materials for a wider range of applications.

Biomorphic silicon carbide (bioSiC) is a SiC-based material fabricated by reactive melt infiltration of molten silicon into carbonaceous preforms obtained from wood pyrolysis [1–6]. The resulting material has a microstructure that resembles that of the original wood precursor, with open porosity often filled by residual Si [7]. BioSiC materials exhibit good thermo-mechanical properties [8]. Its properties are highly anisotropic and depend on the microstructure, which in turn depends on the structure of the wood precursor. Therefore, by careful selection of the precursor properties (mainly density and pore size distribution), a whole range of bioSiC ceramics can be easily fabricated with properties tailored to each particular application [9, 10].

BioSiC ceramics also have other advantages. The carbonaceous precursor can be machined to near net-shape prior to infiltration, thus reducing manufacturing cost by avoiding expensive cutting and machining processes on the SiC. Numerous applications have already been suggested for these materials, such as heating elements, high-temperature absorbers [11], and medical implants for bone substitution [12].

However, for the implementation of these materials to be feasible, a wider understanding of the processes involved during the fabrication stage is needed. In particular, knowledge of the infiltration and reaction–formation mechanisms in terms of the microstructure and pore size distribution of the carbon precursors is essential. Previous attempts to elaborate a model for the fabrication processes, although successful, do not explain completely the microstructural features found in bioSiC [13].

F. M. Varela-Feria · J. Ramírez-Rico (✉) ·
A. R. de Arellano-López · J. Martínez-Fernández
Departamento de Física de la Materia Condensada-ICMSE, Universidad de Sevilla-CSIC, P.O. Box 1065, 41080 Sevilla, Spain
e-mail: jrr@us.es

M. Singh
Ohio Aerospace Institute, NASA Glenn Research Center, Cleveland, OH 44135, USA

This work represents an attempt at explaining the infiltration and reaction–formation of SiC mechanisms that dominate the fabrication process of bioSiC. The infiltration kinetics will be explained in terms of the microstructure of the carbonaceous preforms, and an estimation of the time needed for complete infiltration will be presented. The microstructure of bioSiC will be described and its origin explained in terms of the possible SiC formation mechanisms. Finally, a model for the microstructural evolution will be presented.

Experimental

BioSiC samples made from Beech (*Fagus* sp.) precursors were fabricated by reactive infiltration of molten Si using a technique, described elsewhere [7]. In brief, wood specimens were cut to near net-shape and pyrolyzed at 1,000 °C (0.5 °C/min heating rate) in flowing Ar. The resulting carbon perform was then infiltrated with liquid Si in excess at 1,450 °C (10 °C/min heating rate) in vacuum. The resulting bioSiC material was then cut using a diamond saw and samples were prepared for SEM and TEM observation using conventional metallographic techniques.

EBSD measurements

BioSiC SEM samples were observed using electron backscattering diffraction (EBSD). Sections longitudinal and transverse to the wood's channels were prepared using conventional metallographic techniques that involved sectioning, grinding, and polishing using diamond paste. The observations were carried out using a TSL-Digiview (EDAX) camera in a Philips XL-30 SEM, and the analysis was performed using OIM Analysis 3.5 Software.

The EBSD technique has been described elsewhere [14–20]. In brief, the electron beam of a SEM is diffracted by the sample surface when tilted adequately. The resulting diffraction pattern is called a Kikuchi pattern and can be recorded in a phosphor screen using a digital camera and indexed using a computer program to calculate the orientation of the sample volume that is interacting with the beam. By using the scanning capabilities of a SEM, thousands of equidistant points in the sample surface can be measured automatically, generating orientation maps in which crystallographic data is spatially resolved.

Infiltration-reaction kinetics

The infiltration-reaction kinetics was studied by measuring the SiC, Si, and residual C contents as a function of infiltration time. Eight pyrolyzed samples of similar shape and weight were infiltrated with excess liquid Si in a Si/C molar ratio of 1.82, at a temperature of 1,450 °C in vacuum for different times ranging from 1 min to 16 h. After the infiltration, a transverse slab was cut from the center of each sample for composition measurements. The slabs were ground to a powder and weighted. Later unreacted Si was etched with a HF and HNO_3 solution according to the reaction:

$$3Si + 12HF + 4HNO_3 \rightarrow 3SiF_4 + 4NO + 8H_2O$$

In the last step residual C was removed from the powders by heating the powders up to 500 °C in atmospheric air. The final powder was found to be composed of only β-SiC by X-ray diffraction, although the presence of a small amount of α-SiC has been reported in similar materials where the processing parameters differed from ours [21]. After each step, the powder was weighted to determine each phase contents.

Results and discussion

Infiltration mechanisms

Figure 1 shows SEM micrographs of carbon precursors from beech. The pores follow a bimodal distribution, with small pores with diameters ranging from 4 to 9 μm and large pores ranging from 30 to 100 μm, depending on the precursor [22]. Molten Si infiltrates into the porous preform by effect of the capillary pressure [23–26]. Jurin's law establishes that the maximum height a liquid can penetrate inside a capillary is:

$$h_{\max} = \frac{2\sigma\cos\theta}{rg\rho} \quad (1)$$

where σ is the surface tension of the liquid, r is the capillary radius, θ the contact angle, g is gravity's acceleration, ρ the liquid's density and $h_{\max}$ is the maximum height of the liquid inside the capillary. In order to describe the dynamical aspects of the liquid's infiltration in the tubular capillary a laminar flow is assumed, so Poiseuille's law can be applied, giving:

$$t = \frac{8\eta}{r^2\rho g}\left[h_{\max}\ln\left[\frac{h_{\max}}{h_{\max}-h}\right] - h\right] \quad (2)$$

where η is the liquid's viscosity, t is the time and h the height of the liquid inside the capillary. With these results an estimation of the maximum infiltration height can be done using the physical properties of molten Si [24, 27, 28]. A carbon preform with a mean pore diameter of 5 μm can be infiltrated with liquid Si up to approximately 25 m high, using a contact angle in the range of $\theta = 0-22°$ for liquid Si versus carbon. Clearly the infiltration process is very fast. For instance, a carbon preform with pore

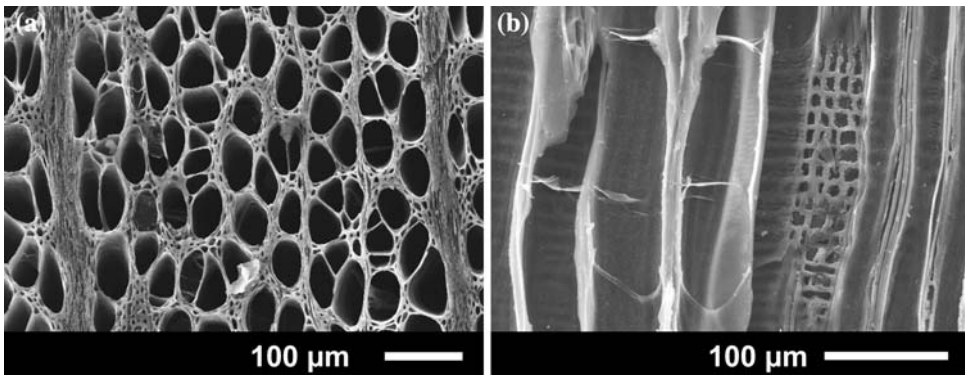

Fig. 1 Low magnification SEM micrographs of bioSiC precursors obtained from Beech. (**a**) Transverse section. (**b**) Longitudinal section

diameters ranging from 5 to 100 µm will be infiltrated in less than 2 s. Although the large channels are infiltrated faster than small ones (due to viscosity effects), the capillary pressure is much larger in the small channels, so because a large channel is connected to some small channels (see Fig. 1b), these will extract liquid Si from the large one until a pressure equilibrium is reached. This explains why the majority of small channels are filled with residual Si, while some of the largest may be not (Fig 2a).

BioSiC microstructure

Figure 2 shows the main microstructural features in bioSiC, as well as the phases observed, which are: residual crystalline Si with bright contrast in SEM micrographs (a–c), polycrystalline SiC and amorphous C, which is normally found in very small quantities. The microstructure of bioSiC presents a bimodal grain size distribution consisting on both micron-sized grains and nanometer-sized grains. SiC grains in the micron range are only found inside channels where Si is majority (large channels with diameter over 5 µm). In small channels where Si is usually depleted in the reaction, SiC grains in the nanometer scale can be observed between the large SiC grains and the unreacted carbon. In general, micron-sized SiC is majority. Normally a layer of micron-sized SiC is formed, where carbon walls previously existed surrounding the large channels. In this case, no nanosized SiC is found. Occasionally this layer is discontinuous and even some isolated SiC grains are observed (Fig. 2b, marked with arrows). Inside small channels micron-sized SiC grains are found

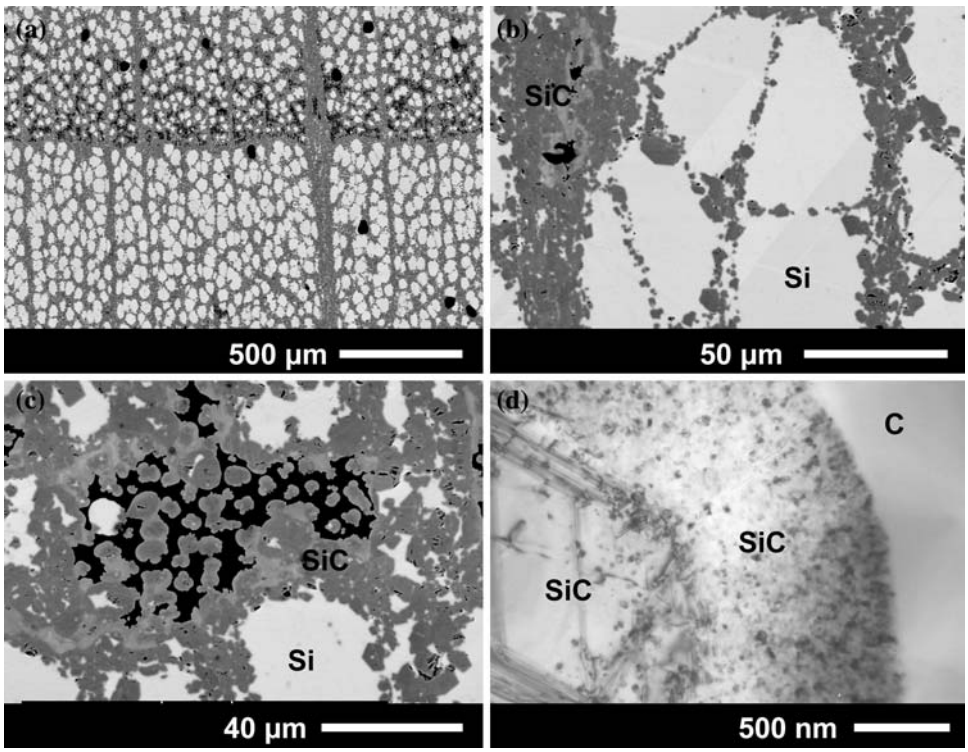

Fig. 2 (**a**) Low magnification SEM micrograph of a bioSiC ceramic obtained using Beech as a precursor. (**b**) High magnification detail of a zone of large channels. (**c**) High magnification detail of a zone of small channels. (**d**) TEM micrograph showing a micrometric SiC grain surrounded by nanosized grains

closing the pores. Surrounding these and towards the unreacted C nanosized grains can be found forming rosettes in certain places, which is typical of diffusion-controlled growth [29], while micron-sized SiC grains are faceted. Both unreacted Si and C areas can be found, normally separated by a SiC layer that prevents further reaction.

Previous observations suggest two cases, depending on the diameter of the channels in the carbon preform. In both cases molten Si penetrates through the carbon preform by capillary effects and reacts with the solid C spontaneously and exothermically, with an enthalpy of $\Delta H^0 = -117.77$ kJ/mol [30]. If the channel is large and Si abundant Si–C groups are formed in Si solution until it saturates and micrometric SiC grains precipitate. In the small channels the process is similar, but the large, micron-sized SiC grains that precipitate close the pores. In these conditions for Si to react with the carbon preform it must diffuse through the SiC layer already formed, thus nanometer-sized SiC grains are formed in a process controlled by diffusion.

EBSD

It is well known that the EBSD technique has a good angular sensitivity, but the measurements of *d*-spacing are of poor precision. This precludes the use of this technique to distinguish phases that have similar crystal structures. In particular, it is not possible for the indexing software to distinguish cubic phases that only differ in their lattice parameters, as is the case with Si and β-SiC. Although during the EBSD data acquisition it was possible to manually attribute each diffraction pattern to one of the two phases, this is not a reasonable option when more than 10^5 diffraction patterns are to be acquired and indexed. The Image Quality (IQ) of an EBSD pattern is defined as the average intensity of the diffracted bands in the pattern that were used for the orientation calculation, and depends on a variety of factors including sample preparation and etching, beam conditions, lattice orientation and crystal structure. Therefore, its absolute value cannot be used for comparison between different materials or even between different samples of the same material. It can, however, give valuable information when relative values are compared within the same dataset. In particular, EBSD patterns from Si yield a higher IQ value than those from SiC in the same dataset due to the differences in density, in very much the same way Si and SiC can be distinguished in SEM using backscattered electron imaging, as in Fig. 2. With these considerations, a generic fcc lattice was selected for the indexing routine, which automatically calculated the orientation of every analyzed point, and then a phase was assigned to every point using an IQ criterion. Figure 3 shows one of the acquired IQ maps for a longitudinal section of bioSiC, where the different phases can be visually distinguished: dark gray corresponds to β-SiC, which has a smaller electron backscattering cross-section, while light gray corresponds to Si. The black areas in the figure correspond to unreacted amorphous C, which could not be indexed by the software and was therefore assigned a zero IQ value. With this criterion, the β-SiC volume fraction could be calculated from the IQ maps, yielding a value of 55% β-SiC which is comparable to the value of 51% calculated using the data from weight analysis (see below). The determination of phase fractions from IQ maps obtained using EBSD is inherently non-precise, but the reasonable agreement between EBSD and composition data validates our approach to separate both crystallographic phases in our analysis. EBSD maps of transverse sections gave similar information, although they are not shown here.

Several interesting features can be observed in Fig. 3: the residual Si that fills the wood channels is in single crystal form, with constant orientation along a channel, although the orientation of Si in every channel was found to be random. Some twins could be observed, both in Si and β-SiC. In Fig. 4a the {100} pole projections of all β-SiC grains present in the map of Fig. 3 are plotted, and the orientation of the residual Si is presented in Fig. 4b. It is clear that the orientation of the β-SiC grains is random and that there is no orientation relation between the residual Si and the β-SiC grains.

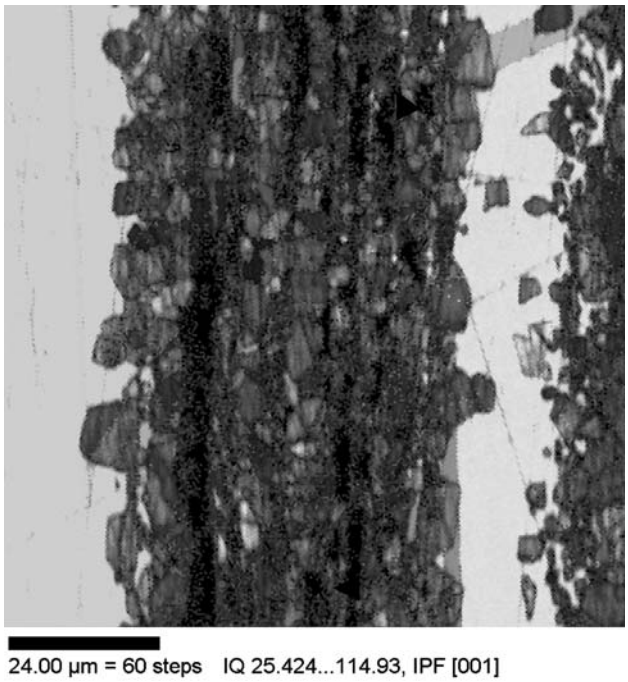

Fig. 3 Image Quality map acquired using EBSD. The C, Si and SiC phases can be clearly distinguished

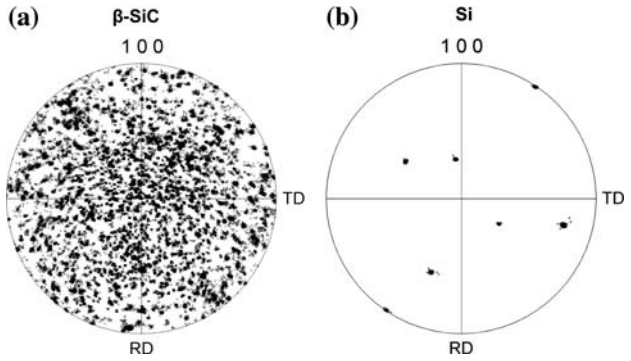

Fig. 4 {100} pole figures of: (**a**) the SiC grains and (**b**) the residual Si calculated using the data from the map shown in Fig. 3

Greil et al. [21] measured the orientation of eight distinct SiC grains surrounding a tracheidal pore in a bioSiC sample (the wood precursor was unreported) and found a preferential orientation of the SiC grains with respect to the axial direction of the wood channels, which was explained by heteroepitaxial growth of SiC at the pore walls. In their view, the pyrolyzed carbon has a graphite-like sheet structure oriented in such a way that the cell walls are hexagonally faceted and approximately coincide with (0001) graphite planes. The existence of this preferential orientation was claimed to be consistent with a diffusion controlled mechanism.

Our EBSD data, on the other hand, show no preferential orientation of the SiC grains, in agreement with TEM observations by Zollfrank and Sieber [13]. This is consistent with a solution–precipitation mechanism in which SiC grains precipitate from a C-rich Si melt after solution of the C layer.

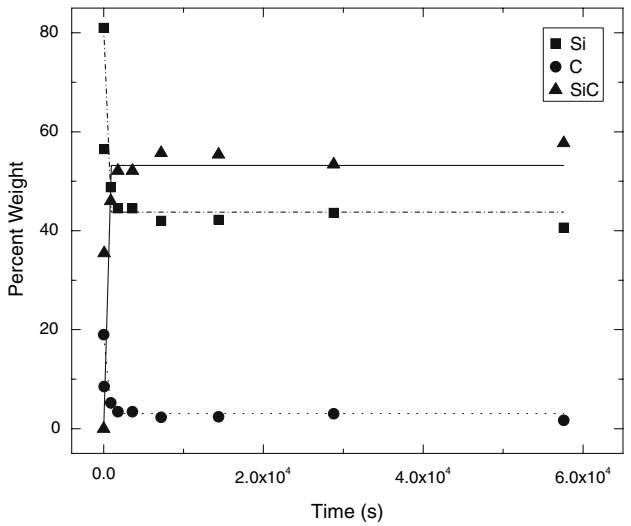

Fig. 5 BioSiC composition as a function of infiltration time

SiC formation mechanisms

Most authors agree in the existence of an initial stage where the surface carbon is dissolved in the liquid Si and then is nucleated as SiC in the carbon surface. The latter growth of SiC can then be controlled by two different mechanisms. One of them is the diffusion of C and/or Si through the previously formed SiC, as described by Hon et al. [29, 31], Fitzer et al. [32, 33] and Zhou and Singh [34]. The other possible process is the solution–precipitation of all the carbon present in the silicon, as described by Pampuch et al [35, 36]. Whether one mechanism or the other dominates will depend on the morphology of the carbon preform. On bulk, pore-less carbon once the initial SiC layer is formed Si and/or C will have to diffuse through the SiC in a slow process, due to the low C and Si diffusion coefficients in SiC [29, 31, 37–39]. Typically, the formation of a 10 μm thick SiC layer takes about 1 h at 1500 °C.

The β-SiC formation reaction follows first order kinetics, so the concentration of each phase can be modeled using:

$$[C_i] = [C_i^f] + ([C_i^0] - [C_i^f])\exp(kt) \quad (3)$$

where k is the reaction constant of the SiC formation reaction and C_i is the concentration of phase i. C_i^f is the concentration of each phase for an infinite reaction time, which has to be introduced since Si is in excess in the process, and C_i^0 is the initial concentration of phase i. Figure 5 shows the measured weight percent of all three phases as a function of time, along with the fits using Eq. 3. The results of the fit are included in Table 1.

Pampuch et al. studied the SiC formation process by reaction of bundles of C fibers 4–6 μm in diameter with liquid Si at 1,422 °C and 1,439 °C [35, 36], and determined the reaction constant k using DTA analysis. They also estimated the reaction constant using diffusion data from Hon et al. [29, 31] and assuming the reaction was controlled by diffusion through the SiC layer, concluding that the reaction had to be controlled by solution–precipitation of the C in the molten Si, as diffusion estimations gave much lower reaction rates than observed. Their results and estimations are presented in Table 2 and compared with the value of the reaction constant as measured in this work.

For porous carbon preforms with wall thickness smaller than 10 μm the diffusion mechanisms play no significant role. Instead the carbon is dissolved in the molten silicon and precipitated as silicon carbide near the carbon walls when the solution supersaturates. In the wood based carbon precursors used for bioSiC the carbon wall thickness is about 2 ± 1 μm, so the SiC formation should be controlled by solution–precipitation exclusively. However, as some of the channels in the preform have a diameter of the same

Table 1 Fit parameters for the data shown in Fig. 5

Phase	$[C_i^0] - [C_i^f]$ (wt.%)	C_i^f (wt.%)	k (10^{-3} s^{-1})
Si	37 ± 3	44 ± 1	18 ± 3
C	16 ± 1	3.0 ± 0.4	18 ± 3
SiC	−53.2 ± 4	53.2 ± 4	18 ± 3

Table 2 Reaction constants as measured by Pampuch et al. [35, 36] and comparison with this work

Temperature (°C)	Reaction constant k (s^{-1})		
	Diffusion controlled process	Solution–precipitation controlled process	This work
1,422	$1.0–2.7 \times 10^{-10}$	0.9×10^{-2}	–
1,439	$1.2–3.3 \times 10^{-10}$	1.7×10^{-2}	–
1,450	–	–	1.8×10^{-2}

range as the wall thickness, they can be closed as the SiC precipitates and thus coalesce with surrounding small channels, yielding an effective SiC layer that is significantly thicker, forcing a scenario where the SiC growth only can happen by a diffusion mechanism. This is also suggested by the presence of unreacted C in bioSiC (Fig. 2c).

Mechanism of carbon solution in liquid silicon

In this scheme, the liquid Si must dissolve the cell walls of the carbon preform to form a solution which will then precipitate as micron-sized SiC grains. An estimation of the time required for the solution of the preform into the molten Si can be made using the Nerst–Noves–Whitney equation:

$$-\frac{dm_c}{dt} = \frac{DA(c_s - c_0)}{\zeta(t)} \tag{4}$$

In Eq. 4 $-dm_c/dt$ is the carbon mass dissolved into the molten Si per unit time, D is the diffusion coefficient of carbon in liquid Si for a given temperature, A is the C–Si(L) contact surface, $\zeta(t)$ is the thickness of the solution layer, c_s is the carbon concentration and c_0 is the initial carbon concentration, which is zero as initially the molten Si contains no C. For our considerations and based on microstructural evidence, we will assume an initial wall thickness of 1 μm and will suppose that the temperature is constant through the C/Si interface and its surroundings, due to the high thermal conductivity of molten Si [40]. We will also suppose that the carbon concentration at the interface is that of equilibrium at the reaction's temperature, that is, $c_s = c_e$ for all $t \geq 0$, being c_e the equilibrium concentration. Also, we will approximate $\zeta(t) \sim 4(Dt)^{1/2}$ [41]. Substituting into Eq. 4, one obtains:

$$\frac{-dm_c}{dt} = \frac{D(T)Ac_e}{4\sqrt{Dt}} = \frac{\sqrt{D(T)}Ac_e}{4\sqrt{t}} \tag{5}$$

Equation 5 allows us to estimate the time needed to dissolve a with 1-μm-thick carbon wall as a function of temperature T. For our calculations c_e has been taken from the works of Scace and Slack [42] and D has been taken from Gnesin and Raichenko [43]. It has been shown that the heat generated by the reaction can raise the temperature in the reaction zone by about 500 °C. This has been observed by Pampuch et al. [35, 36] by Differential Thermal Analysis of the infiltration and reaction process of molten Si in a preform made of carbon fibers, and by Sangsuwan et al. [26]. Therefore, if the molten Si temperature is 1,550 °C, then the process can reach 2,000 °C inside the C preform. For this temperature, and considering a wall thickness of 1 μm all the carbon of the wall is dissolved in about a minute.

Reaction–formation mechanism and microstructural evolution

We propose a model for the formation of bioSiC based in the C–Si phase diagram, as shown in Fig. 6. If Si is majority then a liquid solution of Si/SiC is formed and micrometric SiC is precipitated upon cooling or saturation of the solution. Wherever C is majority, there is no Si/C liquid interface and the SiC is formed by a diffusion process that yields nanosized SiC grains. Whatever one or the scenario happens depends mainly on the channel diameter.

In Fig. 7 schematics of the SiC formation inside the large channels are shown, where liquid Si is majority.

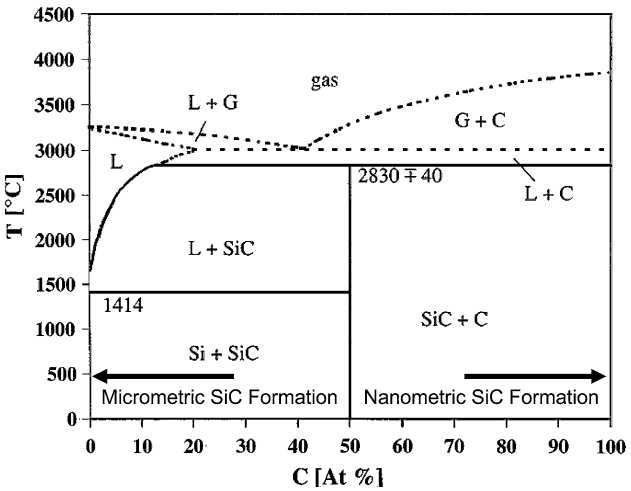

Fig. 6 Si–C phase diagram [44]

Liquid Si penetrates the carbon preform by capillary forces and because in the preforms the porosity is connected, the molten Si reaches all pores and channels. This process takes place in a few seconds, as has been previously shown. Silicon then reacts with the carbon preform forming Si–C groups dissolved in the liquid by corrosion of the carbon walls that surround the channels. As the walls are 1–2 μm thick, the amount of available C is small compared to the Si volume and C is quickly depleted. This process takes about a minute as has been previously shown.

The solution process is aided by the heat generated during the reaction which in turn raises the liquid Si temperature and enhances the C solubility (left side of the phase diagram, Fig. 6). The phase diagram shows that the SiC/Si supersaturates for small C concentrations, producing the precipitation of SiC near the C walls, yielding SiC grains in the micron range. This is supported by the faceted morphology of the large SiC grains. The process ends when all the carbon is depleted and all SiC has precipitated.

If the channel diameter is comparable to the C wall thickness then the pores can become choked by the precipitation of SiC. In that case the SiC barrier prevents the complete reaction of the C preform in that zone, and so some unreacted C remains in the sample. The process in this scenario is schematized in Fig. 8. As happens when the channels are large, the Si infiltration occurs by means of capillary pressure. The liquid Si then reacts with the C in the preform forming Si–C groups dissolved in the melt. Since there is more carbon than silicon, the solution is supersaturated earlier than in the previous case, and so micron-sized grains precipitate inside the channel and end up choking it. Up to now, the process is similar to the previous scenario and happens in the left part of the phase diagram in Fig. 6. The Si is less and less available as the reaction takes place and so the system is displaced to the right side of the phase diagram (Fig. 6), which is carbon rich. In this zone there is no solubility of Si into C so it is impossible for a solution–precipitation mechanism to occur. The only possibility available to the system is the formation of SiC by diffusion through the already formed SiC layer. At the SiC/C interface the grains have a size in the nanometer range, because the kinetic of the reaction is extremely slow. For practical effects and considering the time the system is allowed to react in typical fabrication conditions, the microstructure is frozen in the first growth stage.

Nanosized SiC was only found at the interfaces between coarse grained SiC and unreacted carbon, for small enough channels. This clearly agrees with our microstructural observations, as can be seen in Figs. 7 and 8. Although other authors have reported different findings regarding this issue, we believe that this can be explained attending to differences in processing parameters. For example, Zollfrank and Sieber [13] find that coarse SiC is always accompanied with nano-SiC until the carbon is depleted, in disagreement with our observations. It is worth noting, however, that their samples were infiltrated at 1,550 °C instead of 1,450 °C as in our case. According to Hon et al. [31], activation energy for self-diffusion of Si in polycrystalline β-SiC is 911 kJ/mol, so the self-diffusion constant is increased by a factor of about 30 when the temperature is increase from 1,450 to 1,550 °C, without even taking into account the temperature increase that

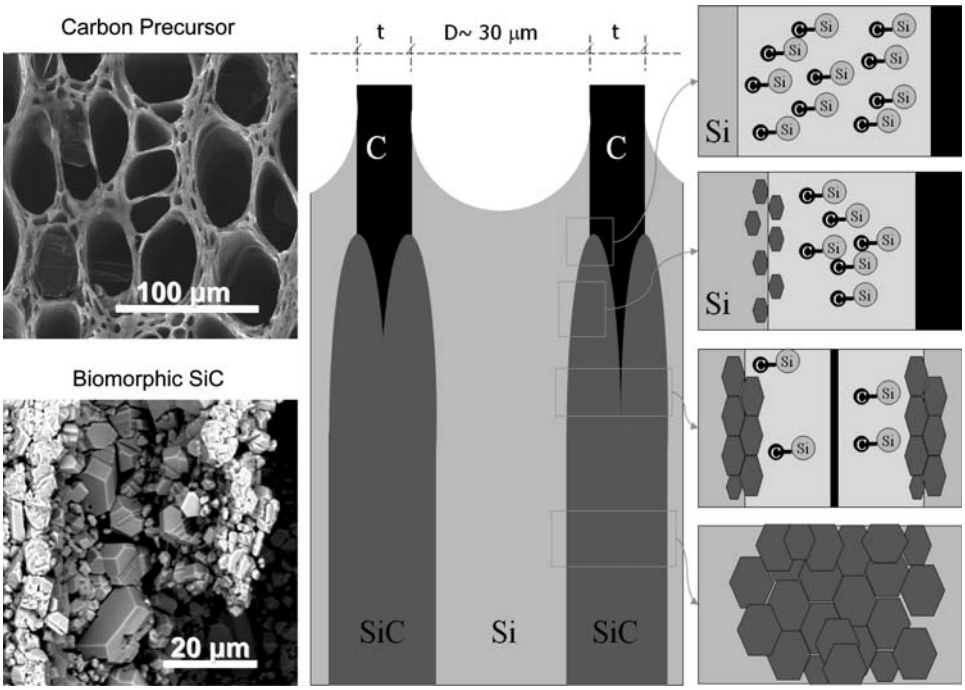

Fig. 7 Infiltration–reaction model in the large channels of the preform

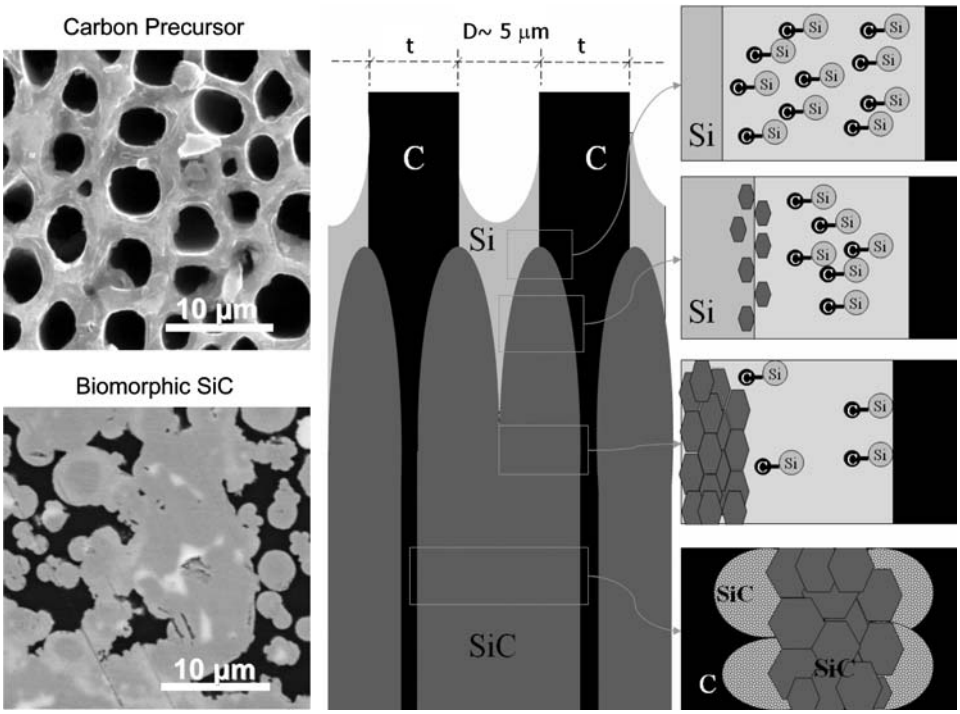

Fig. 8 Infiltration–reaction model in the narrow channels of the preform

accompanies the SiC formation reaction. As previously stated, the two available mechanisms for SiC formation are precipitation and diffusion, the importance of the later being greatly increased at 1,550 °C. This can explain why other authors find nano-SiC in places where we do not. In our case, nano-SiC is only found in places, where precipitation cannot occur, i.e., narrow channels that have been choked by coarse grained SiC.

Conclusions

Biomorphic silicon carbide is fabricated by reactive infiltration of liquid silicon in carbon preforms obtained from wood pyrolysis. The liquid Si infiltrates in the preform by capillary forces, and the time required for this process to be complete has been estimated. The formation mechanisms of SiC have been identified.

The molten silicon reacts with the carbon preform by a spontaneous and exothermic reaction that dissolves the carbon, forming Si–C groups that precipitate as micron-sized SiC. If there is not enough silicon to dissolve the carbon, then the SiC layer formed prevents further reaction and SiC must grow by diffusion processes. These results explain the microstructural features observed and are in good agreement with the works found in literature.

Acknowledgements This work was supported by the Spanish Ministry of Science and Technology through Grant MAT 2006-13005-C. The authors are grateful to the CITIUS at the University of Seville for the use of their electron microscopy facilities. J.R.-R. is grateful to the Junta de Andalucía for his pre-doctoral Grant.

References

1. Martinez-Fernandez J, Varela-Feria FM, Singh M (2000) Scripta Mater 43:813
2. Singh M, Behrendt DR (1994) J Mater Res 9:1701
3. Singh M, Behrendt DR (1995) Mater Sci Eng A 194:193
4. Byrne CE, Nagle DC (1997) Carbon 35:259
5. Byrne CE, Nagle DC (1997) Carbon 35:267
6. Byrne CE, Nagle DC (1997) Mater Res Innov 1:137
7. Martinez-Fernandez J, De Arellano-Lopez AR, Varela-Feria FM, Singh M (2001) Procedimiento para la Fabricación de Carburo de Silicio a partir de Precursores Vegetales. vol. P200102278. Spain
8. Varela-Feria FM, Martinez-Fernandez J, De Arellano-Lopez AR, Singh M (2002) J Eur Ceram Soc 22:2719
9. Varela-Feria FM, Lopez-Robledo MJ, Martinez-Fernandez J, De Arellano-Lopez AR, Singh M (2002) Ceram Eng Sci Proc 23:681
10. Martinez-Fernandez J, Munoz A, De Arellano-Lopez AR, Varela-Feria FM, Dominguez-Rodriguez A, Singh M (2003) Acta Mater 51:3259
11. De Arellano-Lopez AR, Martinez-Fernandez J, Gonzalez P, Dominguez C, Fernandez-Quero V, Singh M (2004) Int J Appl Ceram Technol 1:56
12. Gonzalez P, Serra J, Liste S, Chiussi S, Leon B, Perez-Amor M, Martinez-Fernandez J, De Arellano-Lopez AR, Varela-Feria FM (2003) Biomaterials 24:4827
13. Zollfrank C, Sieber H (2005) J Am Ceram Soc 88:51
14. Coates DG (1967) Philos Mag 16:1179
15. Dingley DJ (2000) In: Schwartz AJ, Kumar M, Adams BL (eds) Electron backscatter diffraction in materials science. Plenum, New York
16. Kocks UF, Tomé CN, Wenk H-R (1998) Texture and anisotropy. Cambridge University Press, Cambridge

17. Randle V, Engler O (2000) Introduction to texture analysis. CRC Press, New York
18. Venables JA, Binjaya R (1977) Philos Mag 35:1317
19. Wright SI, Adams BL (1991) Textures Microstructures 14:273
20. Wright SI, Adams BL (1992) Metall Trans A Phys Metall Mater Sci 23:759
21. Greil P, Lifka T, Kaindl A (1998) J Eur Ceram Soc 18:1961
22. Singh M, Martinez-Fernandez J, De Arellano-Lopez AR (2003) Curr Opin Solid State Mater Sci 7:247
23. Bhagat RB, Singh M (1994) In: Singh M, Lewins D (eds) In-situ composites: science and technology. The Minerals, Metals and Materials Society, p 135
24. Gern FH, Kochendorfer R (1997) Compos Part A Appl Sci 28:355
25. Greil P (2001) J Eur Ceram Soc 21:105
26. Sangsuwan P, Tewari SN, Gatica JE, Singh M, Dickerson R (1999) Metall Mater Trans A 30:933
27. Gerwien ML (1986) In: Warucke R (ed) Gmelin handbook of inorganic chemistry, 8th edn. Springer-Verlag, Berlin
28. Grabmaier J, Ciszek TF (1981) Silicon. Springer-Verlag, Berlin
29. Hon MH, Davis RF (1979) J Mater Sci 14:2411 (DOI: 10.1007/BF00737031)
30. Weast RCE (1974) Handbook of chemistry and physics. CRC Press, Cleveland
31. Hon MH, Davis RF, Newbury DE (1980) J Mater Sci 15:2073 (DOI: 10.1007/BF00550634)
32. Fitzer E, Fritz W, Gadow R (1985) Chem Ing Tech 57:737
33. Fitzer E, Gadow R (1986) Am Ceram Soc Bull 65:326
34. Zhou H, Singh RN (1995) J Am Ceram Soc 78:2456
35. Pampuch R, Bialoskorski J, Walasek E (1987) Ceram Int 13:63
36. Pampuch R, Walasek E, Bialoskorski J (1986) Ceram Int 12:99
37. Hong JD, Davis RF (1980) J Am Ceram Soc 63:546
38. Hong JD, Davis RF, Newbury DE (1981) J Mater Sci 16:2485 (DOI: 10.1007/BF01113585)
39. Hong JD, Hon MH, Davis RF (1979) Am Ceram Soc Bull 58:348
40. Bartlett RW, Nelson WE, Halden FA (1967) J Electrochem Soc 114:1149
41. Crank J (1975) The mathematics of diffusion. Clarendon Press, Oxford
42. Scace RI, Slack GA (1959) J Chem Phys 30:1551
43. Gnesin GG, Raichenko AI (1973) Poroshkovaya Metallurgiya 5:35
44. Kleykamp H, Schumacher G (1993) Ber Bunsen-Ges Phys Chem 97:799